■ Molecular Electronics

Single-Molecule Conductance Studies of Organometallic Complexes Bearing 3-Thienyl Contacting Groups

Sören Bock,[a] Oday A. Al-Owaedi,[b, c] Samantha G. Eaves,[a, d] David C. Milan,[e] Mario Lemmer,[f] Brian W. Skelton,[a, g] Henrry M. Osorio,[h, i, j] Richard J. Nichols,[e] Simon J. Higgins,[e] Pilar Cea,[h, i] Nicholas J. Long,[f] Tim Albrecht,[f] Santiago Martín,*[h, k] Colin J. Lambert,*[b] and Paul J. Low*[a]

Abstract: The compounds and complexes 1,4-C_6H_4(C≡C-*cyclo*-3-C_4H_3S)$_2$ (**2**), *trans*-[Pt(C≡C-*cyclo*-3-C_4H_3S)$_2$(PEt$_3$)$_2$] (**3**), *trans*-[Ru(C≡C-*cyclo*-3-C_4H_3S)$_2$(dppe)$_2$] (**4**; dppe = 1,2-bis(diphenylphosphino)ethane) and *trans*-[Ru(C≡C-*cyclo*-3-C_4H_3S)$_2${P(OEt)$_3$}$_4$] (**5**) featuring the 3-thienyl moiety as a surface contacting group for gold electrodes have been prepared, crystallographically characterised in the case of **3**–**5** and studied in metal|molecule|metal junctions by using both scanning tunnelling microscope break-junction (STM-BJ) and STM-*I(s)* methods (measuring the tunnelling current (*I*) as a function of distance (*s*)). The compounds exhibit simi-

lar conductance profiles, with a low conductance feature being more readily identified by STM-*I(s)* methods, and a higher feature by the STM-BJ method. The lower conductance feature was further characterised by analysis using an unsupervised, automated multi-parameter vector classification (MPVC) of the conductance traces. The combination of similarly structured HOMOs and non-resonant tunnelling mechanism accounts for the remarkably similar conductance values across the chemically distinct members of the family **2**–**5**.

Introduction

The development of a range of complementary and relatively facile methods for the measurement of the electrical properties of single molecules has seen a renaissance in the field of molecular electronics.[1–4] The continued progress of the area from fundamental science towards technology now rests on a number of key issues,[5] among which are the reliable contacting of molecules within a junction,[6,7] the reduction in electronic variation between individual junctions[1,8–12] and the optimisation of the transport properties of these junctions.[13–16] To these ends, considerable effort is being made to explore the effects of the electrode–molecule contact groups and structure of the contact,[17–20] the potential applications of non-metallic

[a] S. Bock, Dr. S. G. Eaves, Prof. B. W. Skelton, Prof. P. J. Low
School of Chemistry and Biochemistry, University of Western Australia
35 Stirling Highway, Crawley, 6009, WA, (Australia)
E-mail: paul.low@uwa.edu.au

[b] Dr. O. A. Al-Owaedi, Prof. C. J. Lambert
Department of Physics, Lancaster University, Lancaster, LA1 4YB (UK)
E-mail: c.lambert@lancaster.ac.uk

[c] Dr. O. A. Al-Owaedi
Department of Laser Physics, Women Faculty of Science
Babylon University (Iraq)

[d] Dr. S. G. Eaves
Department of Chemistry, Durham University
South Rd., Durham, DH1 3LE (UK)

[e] Dr. D. C. Milan, Prof. R. J. Nichols, Prof. S. J. Higgins
Department of Chemistry, University of Liverpool
Crown St., Liverpool, L69 7ZD (UK)

[f] M. Lemmer, Prof. N. J. Long, Prof. T. Albrecht
Department of Chemistry, Imperial College London, London SW7 2AZ (UK)

[g] Prof. B. W. Skelton
Centre for Microscopy, Characterisation and Analysis
University of Western Australia, Crawley, Western Australia 6009 (Australia)

[h] Dr. H. M. Osorio, Dr. P. Cea, Dr. S. Martín
Departamento de Química Física, Facultad de Ciencias
Universidad de Zaragoza, 50009 Zaragoza (Spain)

E-mail: smartins@unizar.es

[i] Dr. H. M. Osorio, Dr. P. Cea
Instituto de Nanociencia de Aragón (INA) y Laboratorio de Microscopias Avanzadas (LMA), Edificio I+D Campus Rio Ebro, Universidad de Zaragoza, C/Mariano Esquillor, s/n, 50018 Zaragoza (Spain)

[j] Dr. H. M. Osorio
Departamento de Física, Escuela Politécnica Nacional
Av. Ladrón de Guevara, E11-253, 170525 Quito (Ecuador)

[k] Dr. S. Martín
Instituto de Ciencias de Materiales de Aragón (ICMA)
Universidad de Zaragoza-CSIC, 50009 Zaragoza (Spain)

electrodes to create an "all-carbon" molecular electronic device platform,[21] as well as the backbone structure of the molecular component on the electrical properties of the junction.[22–24]

Although the majority of single-molecule and thin-film junctions studied to date have been based on organic molecules, such as alkanes,[25,26] oligo(arylene)ethynylenes[27–29] and polyynes,[30–33] metal complexes have also been recognised as potential components in a future molecular electronics technology.[34–38] Metal complexes offer a range of potential advantages over structurally and electronically simpler organic molecules, including redox activity and a wider range of readily accessible and systematically variable spin-states and magnetic properties,[39–42] diversity of molecular structure and potential for modular construction through in situ or "on surface" coordination chemistry,[43–46] better alignment of the frontier molecular orbitals with the Fermi level of the (usually metallic) junction electrodes,[8,47–50] as well as high thermoelectric efficiency.[51]

In some earlier studies of organometallic complexes in molecular electronics, the complex trans-[Pt(C≡CC$_6$H$_4$SAc)$_2$(PPh$_3$)$_2$] was assembled within a mechanically controlled break-junction (MCBJ) based molecular junction. From the resulting I/V curves, collected over a bias range of ±5 V, a resistance of 5–50 GΩ (i.e., $G = 0.2$–0.02 nS; 20–2×10^{-6} G$_0$) was estimated at the extremes of the bias range, some three orders of magnitude less conductive than similarly contacted organic oligoarylene systems.[52] This "insulating" behaviour, even under such a high applied bias, was ascribed to the largely σ-type Pt–C(sp) bonds in the C≡C–Pt–C≡C backbone, although it is clear that at this bias voltage, the conductance mechanism is likely to be field emission rather than tunnelling.[53] In contrast, a later study with a family of complexes of type trans-[Pt(C≡CC$_6$H$_4$SAc)$_2$(L)$_2$] (L = PCy$_3$, PPh$_3$, P(OEt)$_3$) in crossed-wire junctions at more modest bias (up to 1 V) revealed a two- to three-fold higher conductance than 1,4-(4-AcSC$_6$H$_4$C≡C)$_2$C$_6$H$_4$, which was ascribed to the shorter sulfur–sulfur distance in the metal complexes.[54]

In seeking to enhance the wire-like response, significant attention was turned to ruthenium bis(alkynyl) complexes, which are generally thought to offer more significant d–π orbital mixing in the occupied frontier molecular orbitals.[9,34,50,55–57] The thioacetate complex trans-[Ru(C≡CC$_6$H$_4$SAc-4)$_2$(dppm)$_2$] (dppm = 1,1-bis(diphenylphosphino)methane) has been assembled into monolayers and studied within a scanning tunnelling microscope break junction (STM-BJ), with a comparison made to the oligo(phenyleneethynylene) (OPE) compound 1,4-(4-AcSC$_6$H$_4$C≡C)$_2$C$_6$H$_4$ as a benchmark. Extrapolation to single-molecule conductances gave values of 19 ± 7 nS (ca. 2.5×10^{-4} G$_0$) for the ruthenium complex and 3.6 ± 2.0 nS (ca. 4.6×10^{-5} G$_0$) for the OPE. The higher conductance has been attributed to both the shorter molecular length and the extensive Ru(d)–C≡C(π) mixing in the metal complex.[56] These concepts have been extended to other examples of organometallic wires based on group 8 metal centres and the trans-bis(alkynyl) motif, with topics of interest including the exploration of surface contacting groups,[9,50] the inclusion of multiple metal centres along the molecular back-bone[35,47,57] and electronic function beyond that of a simple wire, such as charge storage and gated transistor-like response.[41,58]

One particular advantage of organometallic complexes within the field of molecular electronics lies in the ability to systematically alter the molecular structures of these systems with a fair degree of synthetic ease, which permits a modular approach to molecular designs and a systematic search for structure–property relationships. In seeking to further explore the electrical properties of oligophenyleneethynylene (OPE), and trans-bis(alkynyl) complexes of platinum and ruthenium, we have turned to such a systematic study here. Here, the 3-thienyl moiety,[59–61] which is readily introduced into both organic and organometallic structures, is used as a contacting group for the ready attachment of organic, ruthenium and platinum-based organometallic complexes within Au|molecule|Au junctions and electrical characterisation by using both the I(s)[62] (measuring the tunnelling current (I) as a function of distance (s)) and STM-BJ[63] methods. The conductance results are interpreted with the aid of DFT level calculations and junction simulations.

Results and Discussion

Synthesis and characterisation

The parent alkyne 3-ethynyl thiophene (HC≡C-cyclo-3-C$_4$H$_3$S, **1**) was obtained from the Sonogashira cross-coupling of 3-bromothiophene with trimethylsilylacetylene and subsequent deprotection.[59] Further cross-coupling of **1** with 1,4-diiodobenzene gave 1,4-C$_6$H$_4$(C≡C-cyclo-3-C$_4$H$_3$S)$_2$ (**2**; Scheme 1).[59] The metal complex trans-[Pt(C≡C-cyclo-3-C$_4$H$_3$S)$_2$(PEt$_3$)$_2$] (**3**) was prepared from the Cu^I-catalysed reaction of **1** and [PtCl$_2$(PEt$_3$)$_2$] in NEt$_3$,[64] whilst trans-[Ru(C≡C-cyclo-3-C$_4$H$_3$S)$_2$(dppe)$_2$] (**4**; dppe = 1,2-bis(diphenylphosphino)ethane) was obtained from the one-pot reaction of [RuCl(dppe)$_2$]OTf with **1**, in the presence of either KOtBu or 1,8-diazabicyclo[5.4.0]undec-7-ene (DBU) and TlBF$_4$.[65] Complexes of the general form trans-[Ru(C≡CR)$_2${P(OEt)$_3$}$_4$] have been prepared in moderate yield from reaction of trans-[RuCl$_2${P(OEt)$_3$}$_4$] with an excess of LiC≡CR.[66] The complex trans-[Ru(C≡C-cyclo-3-C$_4$H$_3$S)$_2${P(OEt)$_3$}$_4$] (**5**) was obtained here simply by allowing the reaction of trans-[RuCl$_2${P(OEt)$_3$}$_4$][67] with **1**, KPF$_6$ and NHiPr$_2$ in ethanol to proceed for 12 days at room temperature, with isolation of the desired compound being achieved by precipitation from methanol. The long reaction time was compensated by the simple reaction conditions and work-up, compatibility with alkynes substituted with sensitive functional groups and improved yields. The compounds were each characterised by the usual array of ^{1}H, ^{13}C{^{1}H} and, in the case of **2–5**, ^{31}P{^{1}H} NMR spectroscopies, mass spectrometry and elemental analysis.

Molecular structures

Single crystals of **3**, **4** and **5** suitable for X-ray diffraction were obtained by recrystallisation by slow diffusion of hexanes (**3**, **4**) or EtOH (**5**) into CH$_2$Cl$_2$ solutions of the complexes. Plots of the molecules showing the atom labelling schemes are given in
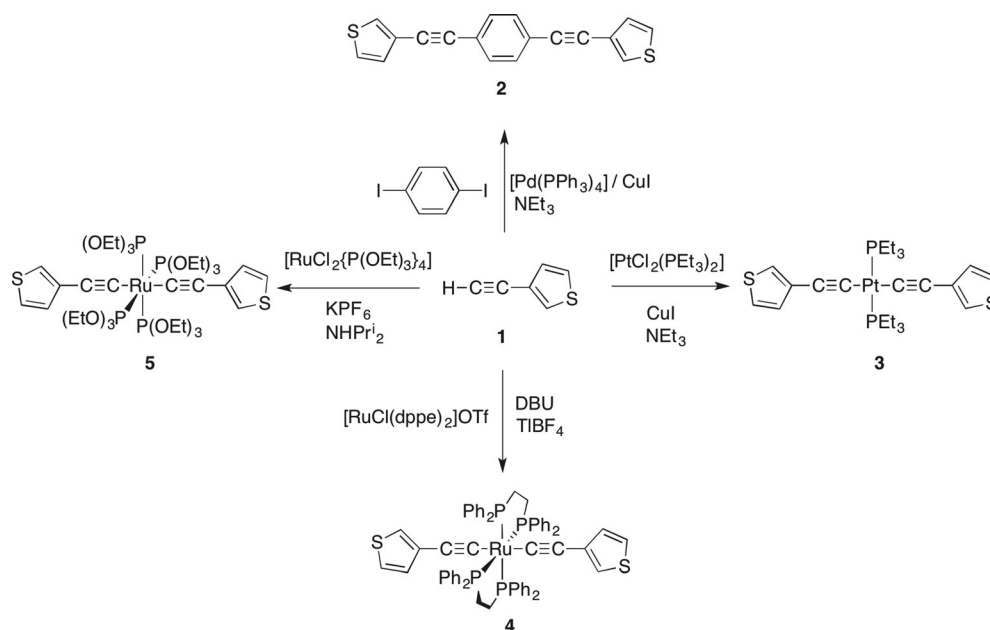
Scheme 1. The preparation of compounds **2**–**5**.

Figures 1, Figures 2 and Figures 3 and the important bond lengths and angles are summarised in the relevant figure captions.

In the crystal, **3** is situated on a crystallographic inversion centre. The platinum atom shows the expected square-planar geometry with *trans*-disposed alkynyl and phosphine ligands. The Pt(1)–P(1) (2.3022(5) Å), Pt(1)–C(1) (2.007(2) Å) and C(1)–C(2) (1.185(3) Å) are all within the usual range of values for complexes of this type,[68] and display little variation of significance with the electronic character of the alkynyl substituent. In the crystal, the P(1)-Pt(1)-C(21)-C(22) torsion angle (136.6°, −43.4°) prevents any significant extended conjugation through the molecule.

The general structural features of *trans*-[Ru(C≡CR)₂(dppe)₂] complexes have been summarised recently,[65] and compound
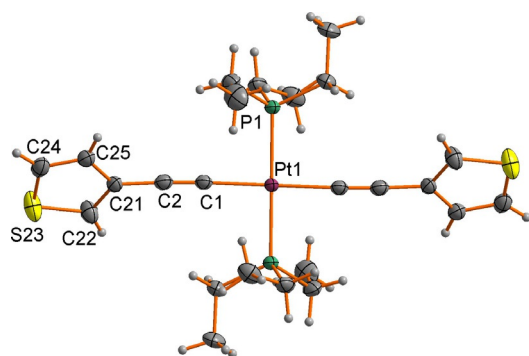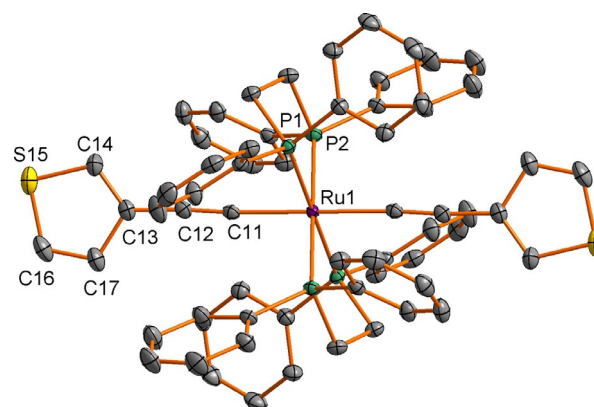

Figure 2. A plot of one molecule of *trans*-[Ru(C≡C-*cyclo*-3-C₄H₃S)₂(dppe)₂] (**4**) (ellipsoids drawn at the 50 % probability level) showing the atom labelling scheme. Bond lengths (molecule 1, Å): Ru(1)–P(1) 2.3539(5); Ru(1)–P(2) 2.3602(5); Ru(1)–C(11) 2.0611(19); C(11)–C(12) 1.218(3); C(12)–C(13) 1.433(3); C(13)–C(14) 1.373(3); C(14)–S(15) 1.709(3); S(15)–C(16) 1.709(3); C(16)–C(17) 1.364(3); C(13)–C(17) 1.448(3). Bond angles (molecule 1, °): P(1)-Ru(1)-P(2) 82.90(2), 97.10(2); P(1)-Ru(1)-C(11) 94.38(5), 85.62; P(2)-Ru(1)-C(11) 97.28(5), 82.72(5); Ru(1)-C(11)-C(12) 176.2(2); C(11)-C(12)-C(13) 176.1(2). Bond lengths (molecule 2, Å): Ru(2)–P(3) 2.3464(4); Ru(2)–P(4) 2.3586(4); Ru(2)–C(21) 2.0626(18); C(21)–C(22) 1.217(3); C(22)–C(23) 1.431(3); C(23)–C(24) 1.389(10); C(24)–S(25) 1.715(10); S(25)–C(26) 1.673(8); C(26)–C(27) 1.352(12); C(23)–C(27) 1.411(10). Bond angles (molecule 2, °): P(3)-Ru(2)-P(4) 97.86(2), 82.14(2); P(3)-Ru(2)-C(21) 96.61(5), 83.39(5); P(4)-Ru(1)-C(21) 84.93(5), 95.07(5); Ru(2)-C(21)-C(22) 177.3(2); C(21)-C(22)-C(23) 176.0(2).

Figure 1. A plot of a molecule of *trans*-[Pt(C≡C-*cyclo*-3-C₄H₃S)₂(PEt₃)₂] (**3**) (ellipsoids drawn at the 50 % probability level) showing the atom labelling scheme. Bond lengths [Å]: Pt(1)–P(1) 2.3022(5); Pt(1)–C(1) 2.007(2); C(1)–C(2) 1.185(3); C(2)–C(21) 1.452(3); C(21)–C(22) 1.373(3); C(22)–S(23) 1.705(3); S(23)–C(24) 1.682(3); C(24)–C(25) 1.393(3); C(21)–C(25) 1.428(3). Bond angles [°]: P(1)-Pt(1)-C(1) 88.32(6), 91.68(6); Pt(1)-C(1)-C(2) 177.83(19); C(1)-C(2)-C(21) 177.3(2).

4 offers some points worthy of brief comment. The structure is composed of two independent molecules, both of which are situated on crystallographic inversion centres and which differ in the orientation of the thiophene group. The dihedral angles between the thiophene plane and the plane containing the Ru and C(n1) atoms and the midpoints of the two ligand P atoms are 3.4° for molecule 1, and 96.3 and 77.8° for the two compo-
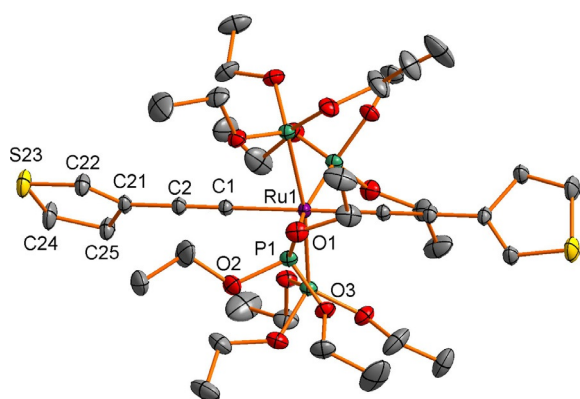
Figure 3. A plot of a molecule (ellipsoids drawn at the 30% probability level) of trans-[Ru(C≡C-cyclo-3-C4H3S)2{P(OEt)3}4] (**5**) showing the atom labelling scheme. Bond lengths [Å]: P(1)–Ru(1) 2.3149(3); Ru(1)–C(1) 2.0592(15); C(1)–C(2) 1.221(2); C(2)–C(21) 1.421(2); C(21)–C(22) 1.36(2); C(22)–S(23) 1.599(12); S(23)–C(24) 1.741(7); C(24)–C(25) 1.480(11); C(25)–C(21) 1.45(2). Bond angles [°]: P(1)-Ru(1)-P(1) 90.338(2), 171.19(2); P(1)-Ru(1)-C(1) 94.40(1), 85.60(1); Ru(1)-C(1)-C(2) 180; C(1)-C(2)-C(21) 180.

nents of the disordered thiophene of molecule 2. Therefore, at least in the crystal, molecules 1 and 2 of **4** are rare examples of such bis(arylacetylide) complexes trans-[Ru(C≡CR)2(dppe)2] in which the aromatic rings sit close to the "privileged" orientations that allow maximum d–π conjugation along the molecular backbone, and the first in which both conformational isomers are observed for the same chemical compound. The comparable bond lengths within the two molecules are essentially indistinguishable, with the possible exception of the most precisely determined Ru–P bond lengths, which appear to be marginally shorter in molecule 2.

Although the mixed ligand vinylidene–acetylide complex [Ru(C≡CPh){C=C(Me)Ph}{P(OEt)3}4][CF3SO3] has been structurally characterised,[66] compound **5** appears to be the first structurally characterised bis(acetylide) derivative of Ru(C≡CR)2{P(OR)3}4. In the crystal, the tetrakis(triethylphosphite) derivative **5** is situated on a crystallographic $\bar{4}$ axis so that there is only one unique phosphite group. The dihedral angle between the two thiophene groups (which are disordered about the crystallographic twofold axis) is therefore 90°. The Ru–P (2.3149(3) Å) and Ru–C(1) (2.0592(15) Å) distances in **5** are shorter than in the mixed vinylidene–acetylide derivative (Ru–P 2.341(3)–2.350(2) Å; Ru–C 2.114(8) Å) reflecting the increased electron density at Ru in **5** and increased Ru–P and Ru–C back bonding. Although back-bonding plays only a modest role in the bonding of metal–alkynyl complexes,[69] the notion is also supported by the trends in C≡C bond lengths in **5** (1.221(2) Å) and the cation [Ru(C≡CPh){C=C(Me)Ph}{P(OEt)3}4]+ (1.209(11) Å). Overall, with the clear exception of the phosphine and phosphite ligands, there are few if any substantive differences in the structures of **4** and **5**.

Single-molecule conductance: STM-BJ and I(s)

Single-molecule conductance measurements were carried out by using substrates with a low surface coverage of the mole-

cules of interest on gold substrates. Low surface coverage was chosen to minimise the formation of multi-molecule junctions and promote formation of single-molecule events. Adsorption of **2**–**5** at low surface coverage was achieved by immersion of a gold-on-glass substrate in CHCl3 solutions of the analyte (1 mм) for about 80 s. After adsorption, the samples were washed in ethanol and then blown dry in a stream of nitrogen. All in situ I(s) and STM-BJ measurements were conducted in mesitylene, a non-polar solvent commonly used in STM-based single-molecule electrical measurements because of its high boiling point and relatively low vapour pressure. For a given set-point current and bias voltage, typically 6000–7000 events were observed in both the STM-BJ and I(s) experiments.

Taking compound **2** as a representative example, without any data selection, it is rather difficult to assign a conductance value to the data (Figure 4). Possible reasons for this include
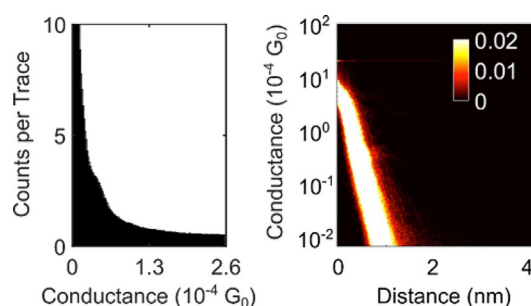

Figure 4. All data 1D (left) and log 2D (right) conductance histograms composed from I(s) data from **2**. Note the 2D histogram is plotted against units of 10^{-4} G0.

a low junction formation probability and short plateau features. The one-dimensional (1D) conductance histogram of the whole data set shows only a faint shoulder, that is, a conductance peak partially obscured by the exponential background (Figure 4, left). Matching the peak, a faint plateau feature can be seen in the 2D conductance histogram (Figure 4, right), but there is a need for data selection for this system to increase signal-to-noise ratio of the data.

Data selection can be made manually, by using a rational criterion, for example by selecting traces with a current plateau that exceeds 0.1 nm in length, and disregarding those without. However, as manual data selection can never be fully objective, it is of interest to compare the results against an automated data selection approach. Here, the unsupervised, automated multi-parameter vector classification (MPVC) has been adopted to verify the conclusions reached from the manually sorted data.[70] By way of example, the data for molecule **2** are analysed in more detail in the following paragraphs, which compare the results of manual and automated data selection methods.

For the MPVC, an exponentially decaying current–distance trace was created as a reference vector, R ($I_0 = 30$ nA, $\beta = 0.5$ Å^{-1}). Three vector properties (classifiers) were then calculated for each I(s) trace with respect to the reference:

1) ΔX: the length of the distance vector, Y, between reference and $I(s)$ trace;
2) θ: the angle, between R and $-Y$;
3) h_r: the reduced Hamming distance, with h_r being the number of component changes to transform the reduced distance vector, Y, into the reduced reference vector, R. In this context, "reduced" means that every vector element is divided by its absolute value, so that the resulting vector consists only of 1, 0 and -1.

The whole data set, consisting of 3838 $I(s)$ traces is thus transformed into 3838 vectors in three-dimensional space (see cylinder plots in the Supporting Information). Here, similar traces, for example, traces with plateaus, are in close proximity to each other. Plain exponential and plateau-containing traces are expected to form distinct clusters in this representation and fuzzy c-means clustering (FCM) was then used to assign the cluster membership.[71,72] Note that the total number of clusters k was selected to be two in this case, to account for plain exponential decays and molecular events, but can be chosen to be a higher number if any cluster consists of sub-clusters (e.g., to account for a variety of different junction geometries).

During FCM, 217 (5.65%) $I(s)$ traces were assigned to cluster 1, containing predominantly exponential decays with plateaus ("molecular events", Figure 5). Cluster 2 contains the remaining, predominantly plain exponential traces (3621, 94.35%; Figure 6). By manual data selection 459 (11.96%) traces were selected as plateau-containing (Figure 7).
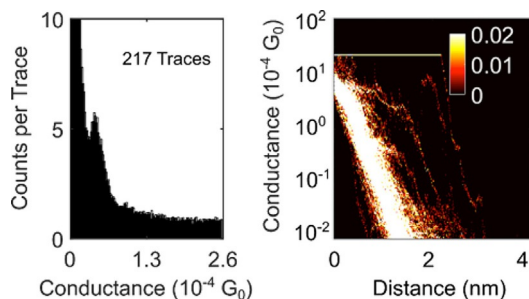

Figure 6. 1D (left) and log 2D (right) conductance histograms of cluster 2, containing predominantly plain exponential traces from **2** without plateaus as found by MPVC. These are assigned to $I(s)$ traces without molecular junction formation.

Figure 7. 1D (left) and log 2D (right) conductance histograms generated by manual selection of data from **2**. Note that the 2D histogram is plotted against units of 10^{-4} G_0.

Figure 5. 1D (left) and log 2D (right) conductance histograms of cluster 1, containing predominantly $I(s)$ traces from **2** with plateaus as found by MPVC. These are assigned to "molecular events" (see main text).

The results of the unsupervised algorithm approach show excellent agreement with the data selected on the basis of the 0.1 nm plateau length criterion described above in terms of conductances, but with understandable differences in terms of number of selected traces. With respect to the latter, some 81 (37.3%) of the plateau traces in cluster 1 were also marked as plateau-containing during the hand-sorting process. Also, 17.6% of the manually selected traces were found by the clustering algorithm. The traces found both by MPVC and hand selection are predominantly long plateaus around the most probable conductance value. In addition, 135 traces were included by the MPVC algorithm but not by hand sorting. These
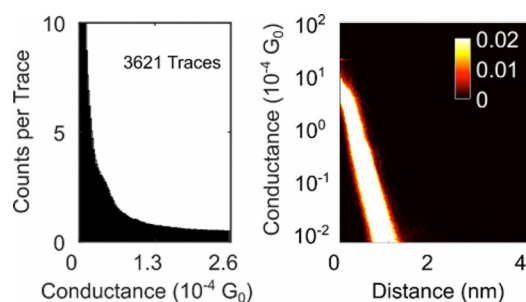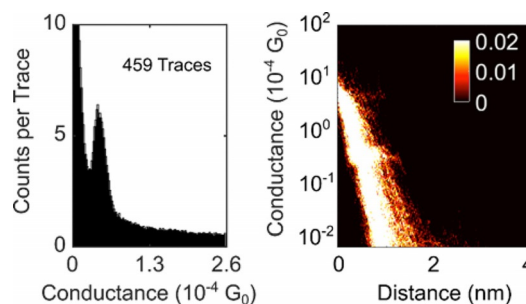
traces contained plateaus at various conductance values or unconventional features, meaning deviations from the plain exponential decay other than plateaus. These can possibly originate from different molecular processes during junction formation (or rupture) or noise features. In contrast, some 377 traces were only marked as plateau-containing during hand selection and not by MPVC. Mostly, those were traces with very short plateau features, or longer plateaus in exponential traces with large decay coefficients. Such features can arise from changes in the molecular junction geometry during the tip retraction process.

After MPVC analysis, cluster 1 exhibits a conductance peak around 0.41×10^{-4} G_0 (Figure 5). Hand sorting gives a most probable conductance of 0.42×10^{-4} G_0 (Figure 7). This indicates that although there are differences in the curve selection between hand sorting and automated sorting, the most probable conductance of both data selection methods shows excellent agreement.

While the non-contact $I(s)$ technique favours low conductance groups,[1] the STM-BJ method generally leads to a greater propensity of higher conductance values. These differences can be explained in terms of the way in which the junctions are formed in both methods. In the $I(s)$ method, the (typically gold) STM tip is brought into close proximity of the surface to encourage molecular junction formation, but without any initial contact between the STM tip and substrate. In contrast, in the STM-BJ technique, the STM tip is fused (or crashed) into

the substrate and withdrawn to give a metallic filament between the tip and the substrate. Molecular junctions form immediately after the Au–Au point contact breaks.[1] The rough or fractal nature of these cleaved gold contact junctions often leads to a variety of conductance features in STM-BJ-based metal|molecule|metal junctions formed from common anchoring groups such as thiol,[1,73] carboxylic acid[74] or pyridine[75] where in each case more than one single molecule conductance value has been reported, and attributed to differing contact morphologies between the contacting groups and the gold electrode(s).

Data recorded by using the STM-BJ technique for compound **2** at $U_{tip} = 0.6$ V are summarized in Figure 8. As shown, the conductance profile from these STM-BJ data for **2** shows only one conductance group (labelled H, for high conductance group). Its most probable conductance ((2.83 ± 0.65) × 10^{-4} G_0, Table 1) is in good agreement with that reported by van der Zant et al. by using the mechanically controlled break-junction (MCBJ) technique (4×10^{-4} G_0).[59]

As shown in Figure 8 and Table 1, distinct conductance groups were also obtained for the metal complexes **3**–**5** by using the I(s) (L group, for low conductance group) and the STM-BJ (H group) method. Interestingly, the compounds **2**–**5** conductance values differ by a factor of about two for the L group, whereas this factor is lower for the H group (Table 1). This demonstrates that the central moiety [C_6H_4 vs. [Pt(PEt$_3$)$_2$] vs. [Ru(dppe)$_2$] vs. [Ru{P(OEt)$_3$}$_4$]] does not exert a great influence on the conductance of these organometallic complexes within these 3-thienyl contacted Au|molecule|Au junctions.

Quantum chemical modelling

In the quest to better understand the conductance behaviour, the electronic properties of the molecules and electrical behaviour of the junctions have been investigated by using DFT-based methods. Initial studies of the electronic structures of **2**–**5** were carried out at the B3LYP level of theory[76] with the LANL2DZ basis set used for metal atoms (Ru, Pt)[77] and the 6-31G**[78] basis set for all other atoms to explore the influence of the central fragment (C_6H_4 (**2**), [Pt(PEt$_3$)$_2$] (**3**), [Ru(dppe)$_2$] (**4**), [Ru{P(OEt)$_3$}$_4$] (**5**)) on the distribution and composition of the frontier molecular orbitals. Plots of the HOMOs are given in Figure 9, and plots of the LUMOs are given in the Supporting Information.

The organic compound **2** again provides a convenient point to commence discussion and a basis for comparison of the metal complexes **3**–**5**. Unsurprisingly, the lowest energy structure features a co-planar arrangement of the thienyl and 1,4-phenylene rings, with the frontier orbitals distributed almost evenly across the molecular backbone, making a linear, π-type conjugated pathway between the two sulfur atoms. For the platinum complex **3**, the lowest energy identified minimum
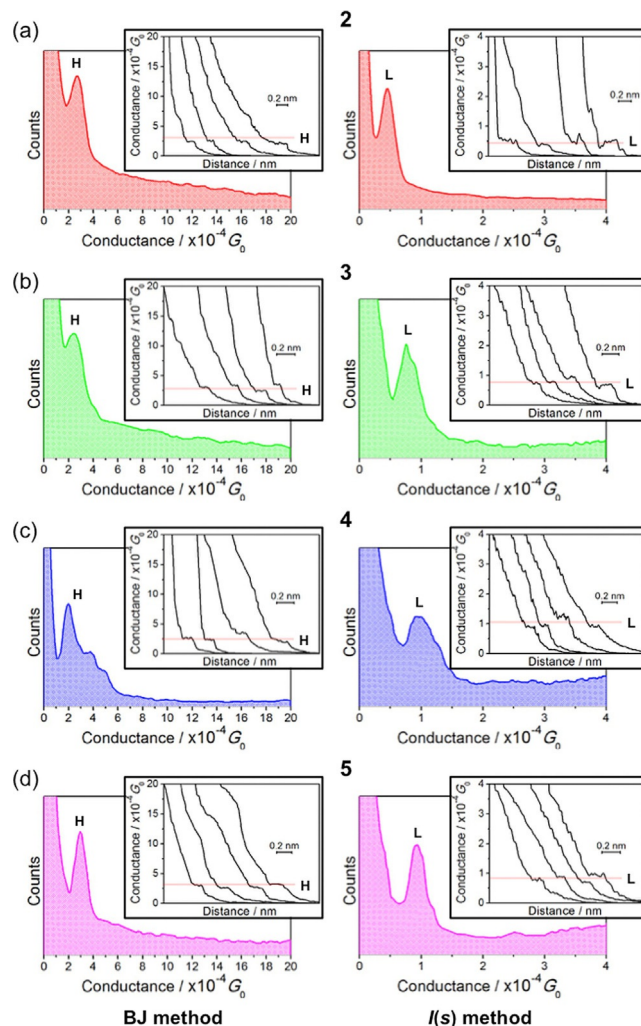

Figure 8. Conductance histograms built by adding all conductance traces (ca. 550) that showed discernible plateaus (with a current plateau that exceeds 0.1 nm in length) as those displayed in the inset of the figures by using either the STM-BJ (left side) or the I(s) method (right side). H = high conductance group. L = low conductance group. a) Compound **2**, b) compound **3**, c) compound **4**, and d) compound **5**. Conductance data are referenced to the conductance quantum $G_0 = 2e^2h^{-1} = 77.5$ μS. $U_{tip} = 0.6$ V.

Table 1. Single-molecule conductance data for compounds 2–5.

	Low conductance (L)[a] [G_0]	High conductance (H)[b] [G_0]	Break-off distance [nm]	Calculated (crystallographic) S···S distance [nm]
2	(0.42 ± 0.10) × 10^{-4}	(2.83 ± 0.65) × 10^{-4}	1.70 ± 0.28	1.60
3	(0.77 ± 0.14) × 10^{-4}	(2.70 ± 0.66) × 10^{-4}	1.85 ± 0.24	1.43 (1.42)
4	(1.03 ± 0.28) × 10^{-4}	(3.18 ± 1.04) × 10^{-4}	1.90 ± 0.24	1.45 (1.44)
5	(0.98 ± 0.14) × 10^{-4}	(3.12 ± 0.58) × 10^{-4}	1.90 ± 0.24	1.45 (1.43)
[a] I(s) method. [b] STM-BJ method.				
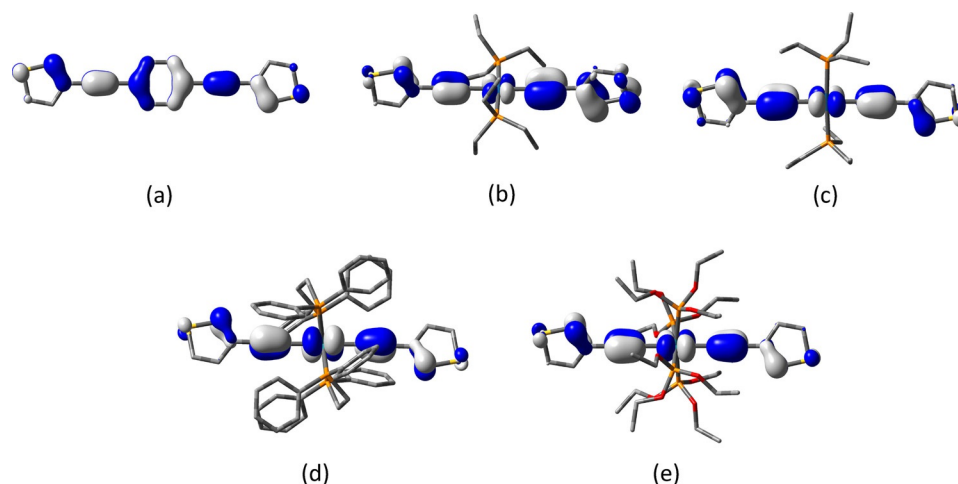
Figure 9. The isosurfaces (± 0.04 (e bohr$^{-3})^{1/2}$) of the HOMOs for: a) **2**, b) perp-**3**, c) planar-**3**, d) **4**, and e) **5**.

featured the thienyl moieties lying perpendicular to the square plane defining the coordination geometry at the metal centre (perp-**3**). However, a second minimum, barely 0.8 kcal mol^{-1} higher in energy, in which the thienyl moieties lie in the same plane as the metal coordination sphere (planar-**3**) was also identified. Again, the HOMOs of these complexes are π-type and delocalized over the molecular backbone, and feature a small but important metal contribution (perp-**3**, 10% Pt; planar-**3**, 19% Pt). The LUMOs are more metal in character (perp-**3**, 42%; planar-**3**, 28%) and rather delocalized in the case of planar-**3**.

The ruthenium complexes **4** and **5** offer HOMOs that are similarly structured to those described for **2** and offer only marginally more metal character than planar-**3** (**4**, 33% Ru; **5**, 24% Ru). The LUMO of **4** is largely of metal/dppe character, in the case of the phosphite analogue **5** the LUMO is thienyl–π* in character, with the unoccupied metal orbital lying slightly (ca. 0.04 eV) higher in energy.

To provide further insight into the experimentally observed trends, and to better evaluate the properties and behaviour of these molecular junctions, calculations using a combination of DFT (the SIESTA code)[79] and a non-equilibrium Green's function formalism were also carried out. For the transport calculations, eight layers of (111)-oriented bulk gold with each layer consisting of 6×6 atoms and a layer spacing of 0.235 nm were used to create the molecular junctions as shown in Figure 6, and described in detail elsewhere.[80] These layers were then further repeated to yield infinitely long current-carrying gold electrodes. Each molecule was attached to two (111) directed pyramidal gold electrodes. The molecules and first layers of gold atoms within each electrode were then allowed to relax again, to yield the optimal junction geometries shown in Figure 10. From these model junctions, the transmission coefficient, $T(E)$, was calculated by using the GOLLUM code.[80]

A key factor governing the conductance of a molecular junction is the position of the Fermi level of a metal electrode with respect to the molecular HOMO and LUMO levels. In turn, this energy alignment is sensitive to not only the chemical nature
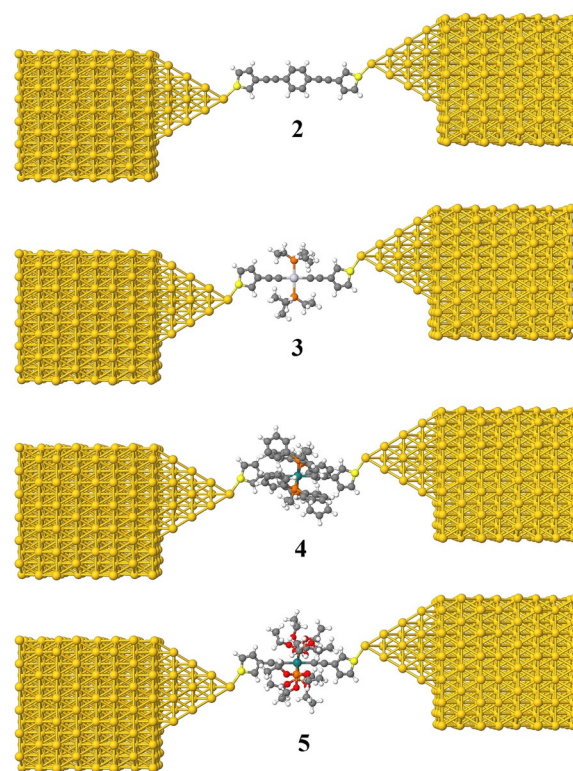

Figure 10. Relaxed geometries of molecular junctions of **2**–**5**.

of the contacting groups that bind the molecule to the electrode, but also the precise configuration of the metal electrode–molecule contact.[15,81] However, it is well known that the Fermi energy predicted by DFT (E_F^{DFT}) is often not reliable,[33] and as such the room-temperature electrical conductance G was computed for a range of Fermi energies E_F. The calculated conductances G are plotted as functions of $E_F-E_F^{DFT}$ in Figure 11, which reveal similar conductance values over a wide range of Fermi energies, between -0.4 eV to $+0.4$ eV relative to the DFT-predicted value. The predicted conductance
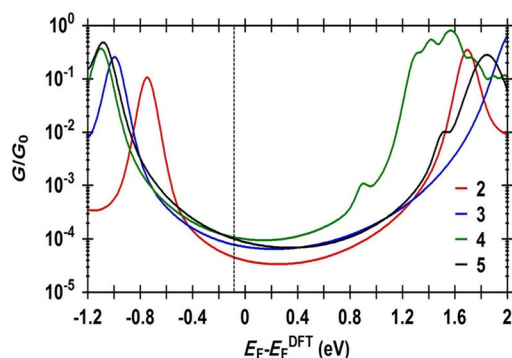
Figure 11. The calculated conductance as a function of the Fermi energy for **2**–**5**. Black dashed line shows the chosen Fermi energy ($E_F = -0.075$ eV).

trons (Q_I) associated with the molecule, the number calculated on the molecule in the junction (Q_{MG}) and hence the number of electrons associated with the thienyl SAu contacts (Γ) (or "bonds") based on calculated Mulliken charges. Mulliken charges are basis-set-dependent mathematical constructions and therefore only approximately coincide with the physical charge on a molecule. However, it is clear from the data in Table 2 that the value of Γ, and the nature of the contact, is only weakly dependent on the nature of the backbone and auxiliary ligands in **2**–**5**. Overall, the molecular conductances of these molecules are similar, with minor variations arising through convolution of the strength of the S→Au bond, and the position of the tail of the HOMO resonance relative to the Fermi level of the electrodes (Table 2).

values of all molecules were compared with the experimental values and a single common value of E_F was chosen, which gave the closest overall agreement. This yielded a small correction of $E_F - E_F^{DFT} = -0.075$ eV, which has been used in all of the theoretical results described below. Thygesen and colleagues have discussed similar situations for C_{60}-contacted molecular wires, and have shown that critical molecular orbitals can become pinned close to the Fermi level owing to partial charge transfer, leading to good quantitative agreement between calculated and experimentally determined conductance.[82]

The experimental data, now interpreted with the aid of Figure 11, indicates that in all cases the Fermi level lies close to the centre of the HOMO–LUMO gap, but shifted slightly towards the HOMO resonance, and therefore a HOMO-mediated hole tunnelling mechanism is anticipated in each case.[47–50,83,84] However, in contrast to the studies of Wang,[56] Rigaut[57] and Mayor[52] with organic, ruthenium and platinum bis(alkynyl) compounds and complexes contacted into molecular junctions by thiolate groups, conductance values only differing by a factor of ≈ 2 are obtained across the thienyl-contacted series **2**–**5**. This lack of variation occurs because although the HOMO and LUMO transport resonances differ significantly between molecules **2**–**5**, transport in the vicinity of the middle of the HOMO–LUMO gap is similar for all molecules (Figure 11).

To further explore the reasons for the small differences in conductance across the series, the nature of the molecule–gold contact was also examined. Table 2 summarises the molecule–gold interaction in terms of the number of valence elec-

Conclusions

The family of 3-thienylethynyl contacted compounds 1,4-$C_6H_4(C{\equiv}C$-*cyclo*-3-$C_4H_3S)_2$ (**2**), *trans*-[Pt(C$\equiv$C-*cyclo*-3-$C_4H_3S)_2(PEt_3)_2$] (**3**), *trans*-[Ru(C$\equiv$C-*cyclo*-3-$C_4H_3S)_2$(dppe)$_2$] (**4**) and *trans*-[Ru(C$\equiv$C-*cyclo*-3-$C_4H_3S)_2\{P(OEt)_3\}_4$] (**5**) have been prepared and studied in metal|molecule|metal junctions by using both STM-$I(s)$ and STM-BJ methods. The compounds **2**–**5** each display two conductance values that differ by a factor of ≈ 2 within the following range of conductance values: (0.44 ± 0.10–1.03 ± 0.28)×10^{-4} G_0 (low conductance group) and (2.70 ± 0.66–3.18 ± 1.04)×10^{-4} G_0 (high conductance group). The MPVC method has been applied to verify the lowest conductance group in an algorithmically definable fashion. For the 3-thienyl contact employed here, the conductance values obtained by using MPVC and manual data selection were very similar, although there were some differences between the current–distance data sets assigned by each method. The MPVC method, which allows reproducible and objective analysis of conductance features close to the limit of the current amplifier, is therefore a promising avenue for the further exploration of low conductance features. In addition, with an increase in the number of sub-clusters the method should also prove useful in the analysis of a wider array of junction configurations or in cases where the junction evolves over time or with distance. Further efforts to develop and exploit the MPVC tool are now underway. A quantum chemical analysis of the electronic structures of the isolated molecules reveals a similarly structured HOMO in each case. Within model junctions, the Fermi level lies slightly towards the HOMO resonance in each case, and

Table 2. The HOMO and LUMO energies of the isolated molecules (eV, c.f. Figure 5), the total number of electrons of the isolated molecule (Q_I), the total number of electrons of the molecule attached to the gold electrodes (Q_{MG}), the total number of electrons transferred from the molecule ($\Gamma = Q - Q_{MG}$) and the calculated and experimental G/G_0.

Molecule	E_{HOMO}	E_{LUMO}	Q_I	Q_{MG}	Γ	Th. G/G_0	Ex. G/G_0 (L group)
2	−5.67	−1.98	94	93.83	0.17	0.45×10^{-4}	0.44 ± 0.10×10^{-4}
planar-**3**[a]	−4.78	−0.71	164	163.775	0.23	0.77×10^{-4}	0.77 ± 0.14×10^{-4}
4	−4.34	−0.87	350	349.696	0.30	1.06×10^{-4}	1.03 ± 0.28×10^{-4}
5	−4.50	−0.08	322	321.672	0.33	0.99×10^{-4}	0.98 ± 0.14×10^{-4}

[a] perp-[**3**] HOMO −4.96 eV, LUMO −0.39 eV.

a non-resonant hole tunnelling mechanism mediated by the similarly structured HOMOs is proposed. The positioning of the Fermi level well within the HOMO–LUMO gap is proposed to account for the similar conductance behaviour across the series. Our study demonstrates that although for some systems, platinum complexes may well be less conductive than purely organic analogues or similarly structured complexes of the group 8 metals, this is not a universal situation, and by appropriate use of contacts and ancillary ligands to position key molecular orbitals with respect to the Fermi levels of the electrodes, rather efficient molecular wires may be engineered. For the future, it will be of interest to study thermal transport through such wires, as although they have similar electrical properties, their vibrational properties and phonon thermal conductances are likely to differ significantly. This ability to tune the latter, while preserving electronic conductance is an attractive proposition for the design of thermoelectric thin films.[85]

Experimental Section

Crystal and refinement data

3: $C_{24}H_{36}P_2PtS_2$, $M = 645.69$, monoclinic, $a = 8.6132(1)$, $b = 11.1767(2)$, $c = 14.1265(2)$ Å, $\beta = 104.958(1)°$, $U = 1313.84(3)$ Å^3, $T = 180$ K, space group $P2_1/n$, $Z = 2$, $\theta_{max} = 36.56°$, 31485 reflections measured, 6229 unique ($R_{int} = 0.034$), $R1 = 0.0230$ $[I > 2\sigma(I)]$, $wR2 = 0.0560$ (all data), $S = 1.068$, $\Delta\rho_{max,min} = 1.509$, -0.775 e Å^{-3}.

4: $C_{64}H_{54}P_4RuS_2 \cdot CH_2Cl_2$, $M = 1197.07$, triclinic, $a = 10.3342(2)$, $b = 13.2414(3)$, $c = 21.4418(5)$ Å, $\alpha = 78.892(2)$, $\beta = 84.176(2)$, $\gamma = 71.219(2)°$, $U = 2723.36(10)$ Å^3, $T = 100$ K, space group $P\bar{1}$, $Z = 2$, $\theta_{max} = 34.38°$, 63208 reflections measured, 21631 unique ($R_{int} = 0.033$), $R1 = 0.0464$ $[I > 2\sigma(I)]$, $wR2 = 0.1100$ (all data), $S = 1.040$, $\Delta\rho_{max,min} = 1.912$, -1.936 e Å^{-3}.

The thiophene group on molecule 2 is disordered over two sites with occupancies constrained to 0.5 after trial refinement. Geometries were restrained to ideal values. Both dichloromethane solvent molecules are disordered about crystallographic inversion centres.

5: $C_{36}H_{66}O_{12}P_4RuS_2$, $M = 979.96$, tetragonal, $a = 11.7879(1)$, $c = 17.5181(3)$ Å, $U = 2432.22(5)$ Å^3, $T = 180$ K, space group $P\bar{4}2_1c$, $Z = 2$, $\theta_{max} = 37.64$, 49278 reflections measured, 6324 unique ($R_{int} = 0.037$), $R1 = 0.0325$ $[I > 2\sigma(I)]$, $wR2 = 0.0746$ (all data), $S = 1.135$, $\Delta\rho_{max,min} = 0.476$, -0.356 e Å^{-3}.

The thiophene group was modelled as being disordered about the crystallographic twofold axis. One methyl group of the triethylphosphite ligand was also modelled as being disordered over two sites with occupancies constrained to 0.5 after trial refinement.

CCDC 1504230 (**3**), 1504231 (**4**), and 1504232 (**5**) contain the supplementary crystallographic data for this paper. These data can be obtained free of charge from The Cambridge Crystallographic Data Centre.

Single-molecule conductance measurements

All single-molecule conductance measurements were recorded at room temperature in mesitylene with an Agilent 5500 SPM microscope. Molecular adlayers were formed on flame-annealed gold on glass samples, purchased from Arrandee, Germany. These commercially available substrates were rinsed with acetone and flame-annealed carefully for about 20 s with a butane torch until a slight orange glow was obtained. This flame-annealing procedure was performed three times and generally resulted in relatively large area flat Au(111) terraces.[86] Gold STM tips were fabricated from 0.25 mm Au wire (99.99%), which was freshly anodically electrochemically etched at +2.4 V for each experiment in a mixture of ethanol (50%) and HCl (50%).

Single-molecule electrical measurements were performed by using both the in situ break-junction (BJ) and $I(s)$ methods. The in situ break-junction method developed by Xu and Tao relies on the formation and cleavage of metallic break junctions between the STM tip and the underlying gold substrate.[63] Such metallic break junctions are formed by forcing the STM tip a certain distance into the gold substrate. The STM tip is then retracted until the gold–gold contact breaks, which leaves an open nanoscale gap into which the molecular targets can adsorb. These molecular bridges then cleave upon further retraction of the STM tip and molecular conductance can be determined by monitoring the current versus distance retraction profiles.

In the $I(s)$ technique, a gold STM tip is brought to a fixed distance, determined by the set point conditions, above the gold surface covered with the target molecule under analysis.[62] Direct metal-to-metal contact between the STM tip and substrate is avoided. The initial approach distance of the STM tip to the substrate surface is controlled by the bias voltage and set-point current (I_0). The measurement involves first locating the STM tip close to the gold substrate at a given height by setting the I_0 and V_{bias} values. The feedback loop of the STM is then temporary disabled and the STM tip is rapidly retracted ($s =$ distance) while the tunnelling current (I) is continuously recorded. At the initial set-point conditions, the target molecules can be trapped between the STM tip and the gold substrate as a molecular bridge. In such circumstances, during the retraction of the STM tip, the molecular bridge is then pulled up and stretched in the nanojunction until the molecular junction is cleaved. For both the BJ and the $I(s)$ methods, when the molecular bridge is formed and then cleaved, a characteristic current plateau is typically observed, with a step-like drop in the current reflecting cleavage of the molecular bridge. On the other hand, if during the tip retraction molecules are not caught in the STM nanogap then the tunnelling current simply decreases exponentially with separation.

Data from the single-molecule studies are available from the University of Liverpool data catalogue (http://datacat.liverpool.ac.uk/187/).

Keywords: contacting group · density functional calculation · organometallic chemistry · scanning tunneling microscopy · single-molecule conductors

[1] W. Haiss, S. Martin, E. Leary, H. van Zalinge, S. J. Higgins, L. Bouffier, R. J. Nichols, *J. Phys. Chem. C* **2009**, *113*, 5823–5833.

[2] F. Schwarz, E. Lortscher, *J. Phys. Condens. Matter* **2014**, *26*, 474201.

[3] C. J. Lambert, *Chem. Soc. Rev.* **2015**, *44*, 875–888.

[4] S. Marqués-González, P. J. Low, *Aust. J. Chem.* **2016**, *69*, 244–253.

[5] a) E. Lörtscher, *Nat. Nanotechnol.* **2013**, *8*, 381–384; b) D. Xiang, X. L. Wang, C. C. Jia, T. Lee, X. F. Guo, *Chem. Rev.* **2016**, *116*, 4318–4440; c) L. Sun, Y. A. Diaz-Fernandez, T. A. Gschneidtner, F. Westerlund, S. Lara-Avila, K. Moth-Poulsen, *Chem. Soc. Rev.* **2014**, *43*, 7378–7411.

[6] J. Hihath, N. J. Tao, *Semicond. Sci. Technol.* **2014**, *29*, 054007.

[7] D. Fracasso, S. Kumar, P. Rudolf, R. C. Chiechi, *RSC Adv.* **2014**, *4*, 56026–56030.

[8] K. Wang, J. Hamill, J. Zhou, C. Guo, B. Q. Xu, *Faraday Discuss.* **2014**, *174*, 91–104.

[9] S. Marqués-González, D. S. Yufit, J. A. K. Howard, S. Martin, H. M. Osorio, V. M. García-Suárez, R. J. Nichols, S. J. Higgins, P. Cea, P. J. Low, *Dalton Trans.* **2013**, *42*, 338–341.

[10] E. Lörtscher, C. J. Cho, M. Mayor, M. Tschudy, C. Rettner, H. Riel, *ChemPhysChem* **2011**, *12*, 1677–1682.

[11] A. Mishchenko, L. A. Zotti, D. Vonlanthen, M. Burkle, F. Pauly, J. C. Cuevas, M. Mayor, T. Wandlowski, *J. Am. Chem. Soc.* **2011**, *133*, 184–187.

[12] I. S. Kristensen, D. J. Mowbray, K. S. Thygesen, K. W. Jacobsen, *J. Phys. Condens. Matter* **2008**, *20*, 374101.

[13] S. Afsari, Z. H. Li, E. Borguet, *Angew. Chem. Int. Ed.* **2014**, *53*, 9771–9774; *Angew. Chem.* **2014**, *126*, 9929–9932.

[14] M. J. Huang, L. Y. Hsu, M. D. Fu, S. T. Chuang, F. W. Tien, C. H. Chen, *J. Am. Chem. Soc.* **2014**, *136*, 1832–1841.

[15] C. C. Jia, X. F. Guo, *Chem. Soc. Rev.* **2013**, *42*, 5642–5660.

[16] M. Kiguchi, S. Kaneko, *ChemPhysChem* **2012**, *13*, 1116–1126.

[17] G. Schull, T. Frederiksen, A. Arnou, D. Sánchez-Portal, R. Berndt, *Nat. Nanotechnol.* **2011**, *6*, 23–27.

[18] C. L. Cheng, R. Skouta, H. Vazquez, J. R. Widawsky, S. Schneebeli, W. Chen, M. S. Hybertsen, R. Breslow, L. Venkataraman, *Nat. Nanotechnol.* **2011**, *6*, 353–357.

[19] Y. Kim, T. J. Hellmuth, M. Burkle, F. Pauly, E. Schneer, *ACS Nano* **2011**, *5*, 4104–4111.

[20] L. A. Zotti, T. Kirchner, J. C. Cuevas, F. Pauly, T. Huhn, E. Scheer, A. Erbe, *Small* **2010**, *6*, 1529–1535.

[21] a) R. McCreery, A. Bergren, A. Morteza-Najarian, S. Y. Sayed, H. J. Yan, *Faraday Discuss.* **2014**, *172*, 9–25; b) C. C. Jia, B. J. Ma, N. Xin, X. F. Guo, *Acc. Chem. Res.* **2015**, *48*, 2565–2575.

[22] N. J. Tao, *Nat. Nanotechnol.* **2006**, *1*, 173–181.

[23] S. V. Aradhya, L. Venkataraman, *Nat. Nanotechnol.* **2013**, *8*, 399–410.

[24] T. A. Su, M. Neupane, M. L. Steigerwald, L. Venkataraman, C. Nuckolls, *Nat. Rev. Mater.* **2016**, *1*, 16002.

[25] X. Y. Feng, Z. Y. Li, J. L. Yang, *J. Phys. Chem. C* **2009**, *113*, 21911–21914.

[26] W. Sheng, Z. Y. Li, Z. Y. Ning, Z. H. Zhang, Z. Q. Yang, H. Guo, *J. Chem. Phys.* **2009**, *131*, 244712.

[27] Y. J. Xing, T. H. Park, R. Venkatramani, S. Keinan, D. N. Beratan, M. J. Therien, E. Borguet, *J. Am. Chem. Soc.* **2010**, *132*, 7946–7956.

[28] L. A. Bumm, J. J. Arnold, M. T. Cygan, T. D. Dunbar, T. P. Burgin, L. Jones, D. L. Allara, J. M. Tour, P. S. Weiss, *Science* **1996**, *271*, 1705–1707.

[29] G. J. Ashwell, B. Urasinka, C. S. Wang, M. R. Bryce, I. Grace, C. J. Lambert, *Chem. Commun.* **2006**, 4706–4708.

[30] P. Moreno-García, M. Gulcur, D. Z. Manrique, T. Pope, W. J. Hong, V. Kaliginedi, C. C. Huang, A. S. Batsanov, M. R. Bryce, C. Lambert, T. Wandlowski, *J. Am. Chem. Soc.* **2013**, *135*, 12228–12240.

[31] A. Al-Backri, V. Zólyomi, C. J. Lambert, *J. Chem. Phys.* **2014**, *140*, 104306.

[32] E. Mostaani, B. Monserrat, N. D. Drummond, C. J. Lambert, *Phys. Chem. Chem. Phys.* **2016**, *18*, 14810–14821.

[33] D. C. Milan, O. A. Al-Owaedi, M.-C. Oerthel, S. Marqués-González, R. J. Brooke, M. R. Bryce, P. Cea, J. Ferrer, S. J. Higgins, C. J. Lambert, P. J. Low, D. Z. Manrique, S. Martin, R. J. Nichols, W. Schwarzacher, V. M. García-Suárez, *J. Phys. Chem. C* **2016**, *120*, 15666–15674.

[34] a) P. J. Low, *Dalton Trans.* **2005**, 2821–2824; b) S. Rigaut, *Dalton Trans.* **2013**, *42*, 15859–15863.

[35] F. Lissel, F. Schwarz, O. Blacque, H. Riel, E. Lortscher, K. Venkatesan, H. Berke, *J. Am. Chem. Soc.* **2014**, *136*, 14560–14569.

[36] J. C. Li, J. Z. Wu, X. Gong, *J. Phys. Chem. Lett.* **2014**, *5*, 1017–1021.

[37] T. Albrecht, A. Guckian, J. Ulstrup, J. G. Vos, *Nano Lett.* **2005**, *5*, 1451–1455.

[38] V. P. Georgiev, P. J. Mohan, D. DeBrincat, J. E. McGrady, *Coord. Chem. Rev.* **2013**, *257*, 290–298.

[39] E. A. Osorio, K. Moth-Poulsen, H. S. J. van der Zant, J. Paaske, P. Hedegard, K. Flensberg, J. Bendix, T. Bjornholm, *Nano Lett.* **2010**, *10*, 105–110.

[40] K. Katoh, H. Isshiki, T. Komeda, M. Yamashita, *Chem. Asian J.* **2012**, *7*, 1154–1169.

[41] F. Schwarz, G. Kaslunger, F. Lissel, C. Egler-Lucas, S. N. Semenov, K. Venkatesan, H. Berke, R. Stadler, E. Lortscher, *Nat. Nanotechnol.* **2016**, *11*, 170–176.

[42] A. C. Aragonès, D. Aravena, J. I. Cerda, Z. Acís-Castillo, H. Li, J. A. Real, F. Sanz, J. Hihath, E. Ruiz, I. Díez-Pérez, *Nano Lett.* **2016**, *16*, 218–226.

[43] H. Masai, J. Terao, S. Seki, S. Nakashima, M. Kiguchi, K. Okoshi, T. Fujihara, Y. Tsuji, *J. Am. Chem. Soc.* **2014**, *136*, 1742–1745.

[44] M. Haga, K. Kobayashi, K. Terada, *Coord. Chem. Rev.* **2007**, *251*, 2688–2701.

[45] R. Sakamoto, S. Katagiri, H. Maeda, Y. Nishimori, S. Miyashita, H. Nishihara, *J. Am. Chem. Soc.* **2015**, *137*, 734–741.

[46] R. Balgley, S. Shankar, M. Lahav, M. E. van der Bloom, *Angew. Chem. Int. Ed.* **2015**, *54*, 12457–12462; *Angew. Chem.* **2015**, *127*, 12634–12639.

[47] F. Schwarz, G. Kastlunger, F. Lissel, H. Riel, K. Venkatesan, H. Berke, R. Stadler, E. Lortscher, *Nano Lett.* **2014**, *14*, 5932–5940.

[48] O. Adak, R. Korytar, A. Y. Joe, F. Evers, L. Venkataraman, *Nano Lett.* **2015**, *15*, 3716–3722.

[49] R. Davidson, O. A. Al-Owaedi, D. C. Milan, Q. Zeng, J. Tory, F. Hartl, S. J. Higgins, R. J. Nichols, C. J. Lambert, P. J. Low, *Inorg. Chem.* **2016**, *55*, 2691–2700.

[50] K. Sugimoto, Y. Tanaka, S. Fujii, T. Tada, M. Kiguchi, M. Akita, *Chem. Commun.* **2016**, *52*, 5796–5799.

[51] H. Nakamura, T. Ohto, T. Ishida, Y. Asai, *J. Am. Chem. Soc.* **2013**, *135*, 16545–16552.

[52] M. Mayor, C. von Hänisch, H. B. Weber, J. Reichert, D. Beckman, *Angew. Chem. Int. Ed.* **2002**, *41*, 1183–1186; *Angew. Chem.* **2002**, *114*, 1228–1231.

[53] G. Frapper, M. Kertesz, *Inorg. Chem.* **1993**, *32*, 732–740.

[54] T. L. Schull, J. G. Kushmerick, C. H. Patterson, C. George, M. H. Moore, S. K. Pollack, R. Shashidhar, *J. Am. Chem. Soc.* **2003**, *125*, 3202–3203.

[55] a) P. J. Low, *Coord. Chem. Rev.* **2013**, *257*, 1507–1532; b) K. Costuas, S. Rigaut, *Dalton Trans.* **2011**, *40*, 5643–5658.

[56] K. Liu, X. Wang, F. S. Wang, *ACS Nano* **2008**, *2*, 2315–2323.

[57] a) F. B. Meng, Y. M. Hervault, Q. Shao, B. H. Hu, L. Norel, S. Rigaut, X. D. Chen, *Nat. Commun.* **2014**, *5*, 3023; b) F. B. Meng, Y. M. Hervault, L. Norel, K. Costuas, C. Van Dyck, V. Geskin, J. Cornil, H. H. Hng, S. Rigaut, X. Chen, *Chem. Sci.* **2012**, *3*, 3113–3118; c) L. Luo, A. Benameur, P. Brignou, S. H. Choi, S. Rigaut, C. D. Frisbie, *J. Phys. Chem. C* **2011**, *115*, 19955–19961; d) B. S. Kim, J. M. Beebe, C. Olivier, S. Rigaut, D. Touchard, J. G. Kushmerick, X. Y. Zhu, C. D. Frisbie, *J. Phys. Chem. C* **2007**, *111*, 7521–7526.

[58] A. K. Mahapatro, J. W. Ying, T. Ren, D. B. Janes, *Nano Lett.* **2008**, *8*, 2131 – 2136.

[59] C. R. Arroyo, S. Tarkuc, R. Frisenda, J. S. Seldenhuis, C. H. M. Woerde, R. Eelkema, F. C. Grozema, H. S. J. van der Zant, *Angew. Chem. Int. Ed.* **2013**, *52*, 3152 – 3155; *Angew. Chem.* **2013**, *125*, 3234 – 3237.

[60] R. G. Nirmal, A. L. Kavitha, S. Berchmans, V. Yegnaraman, *J. Nanosci. Nanotechnol.* **2007**, *7*, 2116 – 2124.

[61] Y. Halpin, H. Logtenberg, L. Cleary, S. Schenk, M. Schulz, A. Draksharapu, W. R. Browne, J. G. Vos, *Eur. J. Inorg. Chem.* **2013**, 4291 – 4299.

[62] W. Haiss, H. van Zalinge, S. J. Higgins, D. Bethell, H. Hobenreich, D. J. Schiffrin, R. J. Nichols, *J. Am. Chem. Soc.* **2003**, *125*, 15294 – 15295.

[63] B. Q. Xu, N. J. Tao, *Science* **2003**, *301*, 1221 – 1223.

[64] K. Sonogashira, Y. Fujikura, T. Yatake, N. Toyoshima, S. Takahashi, N. Hagihara, *J. Organomet. Chem.* **1978**, *145*, 101 – 108.

[65] S. Marqués-González, M. Parthey, D. S. Yufit, J. A. K. Howard, M. Kaupp, P. J. Low, *Organometallics* **2014**, *33*, 4947 – 4963.

[66] G. Albertin, S. Antoniutti, E. Bordignon, F. Cazzaro, S. Ianelli, G. Pelizzi, *Organometallics* **1995**, *14*, 4114 – 4125.

[67] W. G. Peet, D. H. Gerlach, D. D. Titus, *Inorg. Synth.* **1974**, *15*, 38 – 42.

[68] See, for example: a) S. C. Jones, V. Coropceanu, T. Kinnibrugh, T. Timofeeva, J.-L. Bredas, S. R. Marder, *J. Am. Chem. Soc.* **2004**, *126*, 11782 – 11783; b) M. Janka, G. K. Anderson, N. P. Rath, *Organometallics* **2004**, *23*, 4382 – 4390; c) C.-H. Tao, N. Zhu, V. W. W. Yam, *Chem. Eur. J.* **2005**, *11*, 1647 – 1657; d) J. P. Carpenter, C. M. Lukehart, *Inorg. Chim. Acta* **1991**, *190*, 7 – 10; e) C. J. Adams, L. E. Bowen, *Dalton Trans.* **2005**, 2239 – 2240; f) X. Zhao, C. Piliego, B. S. Kim, B. Ma, D. A. Unruh, J. M. J. Frechet, *Chem. Mater.* **2010**, *22*, 2325 – 2332; g) K. Gagnon, S. M. Aly, A. Brisach-Wittmeyer, D. Bellows, J.-F. Berube, L. Caron, A. S. Abd-El-Aziz, D. Fortin, P. D. Harvey, *Organometallics* **2008**, *27*, 2201 – 2214.

[69] J. E. McGrady, T. Lovell, R. Stranger, M. G. Humphrey, *Organometallics* **1997**, *16*, 4004 – 4011.

[70] M. Lemmer, M. S. Inkpen, K. Kornysheva, N. J. Long, T. Albrecht, *Nat. Commun.* **2016**, *7*, 12922.

[71] Fuzzy clustering was performed with the "Clustering and Data Analysis Toolbox" by J. Abonyi available from MATLAB file exchange http://au.-mathworks.com/matlabcentral/fileexchange/7473-clustering-and-data-analysis-toolbox.

[72] D. E. Gustafson, W. C. Kessel, IEEE Conference on Decision and Control, San Diego, CA, **1978**, 761 – 766; DOI: 10.1109/CDC.1978.268028.

[73] C. Li, I. Pobelov, T. Wandlowski, A. Bagrets, A. Arnold, F. Evers, *J. Am. Chem. Soc.* **2008**, *130*, 318 – 326.

[74] S. Martin, W. Haiss, S. J. Higgins, R. J. Nichols, *Nano Lett.* **2010**, *10*, 2019 – 2023.

[75] a) C. S. Wang, A. S. Batsanov, M. R. Bryce, S. Martin, R. J. Nichols, S. J. Higgins, V. M. Garcia-Suarez, C. J. Lambert, *J. Am. Chem. Soc.* **2009**, *131*, 15647 – 15654; b) D. Z. Manrique, C. Huang, M. Baghernejad, Z. Zhao, O. A. Al-Owaedi, H. Sadeghi, V. Kaliginedi, W. Hong, M. Gulcur, T. Wandlowski, M. R. Bryce, C. J. Lambert, *Nat. Commun.* **2015**, *6*, 6389; c) M. Kamenetska, S. Y. Quek, A. C. Whalley, M. L. Steigerwald, H. J. Choi, S. G. Louie, C. Nuckolls, M. S. Hybertsen, J. B. Neaton, L. Venkataraman, *J. Am. Chem. Soc.* **2010**, *132*, 6817 – 6821.

[76] a) A. D. Becke, *J. Chem. Phys.* **1993**, *98*, 5648 – 5652; b) P. J. Stephens, F. J. Devlin, C. F. Chabalowski, M. J. Frisch, *J. Phys. Chem.* **1994**, *98*, 11623 – 11627.

[77] a) P. J. Hay, W. R. Wadt, *J. Chem. Phys.* **1985**, *82*, 270 – 283; b) W. R. Wadt, P. J. Hay, *J. Chem. Phys.* **1985**, *82*, 284 – 298; c) P. J. Hay, W. R. Wadt, *J. Chem. Phys.* **1985**, *82*, 299 – 310.

[78] G. A. Petersson, M. A. Al-Laham, *J. Chem. Phys.* **1991**, *94*, 6081 – 6090.

[79] J. M. Soler, E. Artacho, J. D. Gale, A. Garcia, J. Junquera, P. Ordejon, D. Sanchez-Portal, *J. Phys. Condens. Matter* **2002**, *14*, 2745 – 2779.

[80] J. Ferrer, C. J. Lambert, V. M. Garcia-Suarez, D. Z. Manrique, D. Visontai, L. Oroszlany, R. Rodriguez-Ferradas, I. Grace, S. W. D. Bailey, K. Gillemot, H. Sadeghi, L. A. Algharagholy, *New J. Phys.* **2014**, *16*, 093029.

[81] a) R. Stadler, K. W. Jacobsen, *Phys. Rev. B* **2006**, *74*, 161405(R); b) R. Stadler, *J. Phys. Conf. Ser.* **2007**, *61*, 1097 – 1101.

[82] T. Markussen, M. Settnes, K. S. Thygesen, *J. Chem. Phys.* **2011**, *135*, 144104.

[83] H. M. Wen, Y. Yang, X. S. Zhou, J. Y. Liu, D. B. Zhang, Z. B. Chen, J. Y. Wang, Z. N. Chen, Z. Q. Tian, *Chem. Sci.* **2013**, *4*, 2471 – 2477.

[84] H. Ozawa, M. Baghernejad, O. A. Al-Owaedi, V. Kaliginedi, T. Nagashima, J. Ferrer, T. Wandlowski, V. M. García-Suárez, P. Broekmann, C. J. Lambert, M. Haga, *Chem. Eur. J.* **2016**, *22*, 12732 – 12740.

[85] C. J. Lambert, H. Sadeghi, Q. Al-Galiby, *Comp. Ren. Phys.* **2016**, *10*, 1084 – 1095.

[86] W. Haiss, D. Lackey, J. K. Sass, K. H. Besocke, *J. Chem. Phys.* **1991**, *95*, 2193 – 2196.